
This is an electronic reprint of the original article.
This reprint may differ from the original in pagination and typographic detail.

Zevenhoven, Koos C.J.; Dong, Hui; Ilmoniemi, Risto J.; Clarke, John

Dynamical cancellation of pulse-induced transients in a metallic shielded room for ultra-low-field magnetic resonance imaging

Published in:
Applied Physics Letters

DOI:
[10.1063/1.4906058](https://doi.org/10.1063/1.4906058)

Published: 01/01/2015

Document Version
Publisher's PDF, also known as Version of record

Please cite the original version:
Zevenhoven, K. C. J., Dong, H., Ilmoniemi, R. J., & Clarke, J. (2015). Dynamical cancellation of pulse-induced transients in a metallic shielded room for ultra-low-field magnetic resonance imaging. *Applied Physics Letters*, 106(034101), 1-5. <https://doi.org/10.1063/1.4906058>

This material is protected by copyright and other intellectual property rights, and duplication or sale of all or part of any of the repository collections is not permitted, except that material may be duplicated by you for your research use or educational purposes in electronic or print form. You must obtain permission for any other use. Electronic or print copies may not be offered, whether for sale or otherwise to anyone who is not an authorised user.

Dynamical cancellation of pulse-induced transients in a metallic shielded room for ultra-low-field magnetic resonance imaging

Koos C. J. Zevenhoven, Hui Dong, Risto J. Ilmoniemi, and John Clarke

Citation: *Appl. Phys. Lett.* **106**, 034101 (2015); doi: 10.1063/1.4906058

View online: <https://doi.org/10.1063/1.4906058>

View Table of Contents: <http://aip.scitation.org/toc/apl/106/3>

Published by the [American Institute of Physics](#)

Articles you may be interested in

[Conductive shield for ultra-low-field magnetic resonance imaging: Theory and measurements of eddy currents](#)
Journal of Applied Physics **115**, 103902 (2014); 10.1063/1.4867220

[Type-I superconductor pick-up coil in superconducting quantum interference device-based ultra-low field nuclear magnetic resonance](#)
Applied Physics Letters **104**, 062602 (2014); 10.1063/1.4865497

[Ultra-low field magnetic resonance imaging detection with gradient tensor compensation in urban unshielded environment](#)
Applied Physics Letters **102**, 102602 (2013); 10.1063/1.4795516

[Thermal noise in biomagnetic measurements](#)
Review of Scientific Instruments **67**, 2397 (1996); 10.1063/1.1147514

[Source localization of brain activity using helium-free interferometer](#)
Applied Physics Letters **104**, 213705 (2014); 10.1063/1.4880097

[Note: Magnetic noise from the inner wall of a magnetically shielded room](#)
Review of Scientific Instruments **84**, 056101 (2013); 10.1063/1.4802845

Quantum Design Brings You the Next Generation Magneto-Optic Cryostat

Only be limited by your imagination...

Room Temperature Window
Split-Coil Conical Magnet
Sample Pod
User Wiring Ports

Learn More

Quantum Design
qdusa.com/opticool5

8 Optical Access Ports: 7 Side; 1 Top
Temperature Range: 1.7 K to 350 K
7 T Split-Coil Conical Magnet
Low Vibration: <10 nm peak-to-peak
89 mm x 84 mm Sample Volume
Automated Temperature & Magnet Control
Cryogen Free

Dynamical cancellation of pulse-induced transients in a metallic shielded room for ultra-low-field magnetic resonance imaging

Koos C. J. Zevenhoven,^{1,a)} Hui Dong,^{2,3} Risto J. Ilmoniemi,¹ and John Clarke²

¹Department of Neuroscience and Biomedical Engineering, School of Science, Aalto University, P.O. Box 12200, FI-00076 AALTO, Finland

²Department of Physics, University of California, Berkeley, California 94708-7300, USA

³State Key Laboratory of Functional Materials for Informatics, Shanghai Institute of Microsystem and Information Technology, Chinese Academy of Sciences, Shanghai 200050, China

(Received 7 November 2014; accepted 4 January 2015; published online 20 January 2015)

Pulse-induced transients such as eddy currents can cause problems in measurement techniques where a signal is acquired after an applied preparatory pulse. In ultra-low-field magnetic resonance imaging, performed in magnetic fields typically of the order of 100 μT , the signal-to-noise ratio is enhanced in part by prepolarizing the proton spins with a pulse of much larger magnetic field and in part by detecting the signal with a Superconducting QUantum Interference Device (SQUID). The pulse turn-off, however, can induce large eddy currents in the shielded room, producing an inhomogeneous magnetic-field transient that both seriously distorts the spin dynamics and exceeds the range of the SQUID readout. It is essential to reduce this transient substantially before image acquisition. We introduce *dynamical cancellation* (DynaCan), a technique in which a precisely designed current waveform is applied to a separate coil during the later part and turn off of the polarizing pulse. This waveform, which bears no resemblance to the polarizing pulse, is designed to drive the eddy currents to zero at the precise moment that the polarizing field becomes zero. We present the theory used to optimize the waveform using a detailed computational model with corrections from measured magnetic-field transients. SQUID-based measurements with DynaCan demonstrate a cancellation of 99%. Dynamical cancellation has the great advantage that, for a given system, the cancellation accuracy can be optimized in software. This technique can be applied to both metal and high-permeability alloy shielded rooms, and even to transients other than eddy currents. © 2015 AIP Publishing LLC. [<http://dx.doi.org/10.1063/1.4906058>]

Ultra-low-field (ULF) magnetic resonance imaging (MRI)^{1–7} operates in a static magnetic field B_0 of typically 50–250 μT , four orders of magnitude weaker than that of clinical MRI machines. ULF MRI has potentially attractive advantages for medical applications. At the corresponding low nuclear magnetic resonance (NMR) frequencies, about 2–10 kHz, the longitudinal relaxation time T_1 is strongly influenced by slow molecular dynamics, enhancing the T_1 contrast between different tissues,⁸ for example, tumor and healthy tissue.⁹ This sensitivity is related to that observed in $T_{1\rho}$ -contrast imaging at high fields, also operating at frequencies of a few kHz, which has been used to monitor progression of Alzheimer's and Parkinson's diseases^{10,11} and to determine the elapsed time since a stroke.¹² Another intriguing application of ULF MRI is its combination with multichannel magnetoencephalography (MEG) systems based on Superconducting Quantum Interference Devices (SQUIDs).^{13,14}

The reduction of B_0 , however, substantially decreases the MRI signal amplitude and hence the signal-to-noise ratio (SNR). This reduction is overcome by a combination of two methods. First, the nuclear spins (protons) are prepolarized¹⁵ by a pulse of magnetic field $B_p \gg B_0$, typically 10–100 mT, prior to acquiring the NMR signal. Second, the NMR signal is acquired with a SQUID coupled to an untuned

superconducting input circuit which, in contrast to the tuned circuit used in conventional MRI, gives a frequency-independent response. This combination yields a signal output from the SQUID that is independent of B_0 and scales as B_p . To protect the SQUID from environmental electromagnetic noise, the system is surrounded by a metallic shielded room. For MEG-MRI, this room has layers of high-permeability alloy, whereas for ULF MRI a room made of only aluminum sheets suffices.

The field B_p must be turned off rapidly—typically in 10 ms—to avoid significant decay of the nuclear polarization before signal acquisition. This rapid change of field induces transient eddy currents in nearby conducting objects, most notably the walls of the shielded room. The resultant inhomogeneous magnetic-field transient may both seriously distort the spin dynamics of the sample and exceed the range of the SQUID readout, and must be greatly reduced before one can begin image encoding and acquisition.

At least three approaches to reducing the eddy currents have been demonstrated. Nieminen *et al.*¹⁶ connected their B_p coil in series with a coaxial, counter-wound cancellation coil—of larger diameter—with parameters carefully designed to cancel the magnetic field at the walls of the shielded room. Hwang *et al.*^{17,18} introduced a large number of spatially distributed cancellation coils, each driven by an accurately calculated fraction of the polarizing coil current. In both cases, the cancellation field has precisely the same waveform as the polarizing field. Zevenhoven *et al.*¹⁹ analyzed the physics of

^{a)}Author to whom correspondence should be addressed. Electronic mail: koos.zevenhoven@aalto.fi

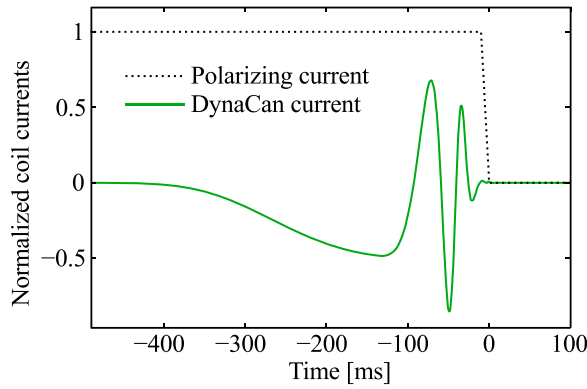


FIG. 1. Dynamical cancellation waveform that cancels the 12 longest time constants in a spherical model system.²⁰ This corresponds to canceling the multipole moments of the B_p coil up to 12th order.

eddy currents in detail to design and construct a shielded room at Berkeley. In a highly symmetric arrangement, selected aluminum plates were separated by resistive layers that reduced the dominant eddy-current decay time constant by one order of magnitude, in agreement with a theoretical model that was presented. This design retains an acceptable level of attenuation of external electromagnetic noise.

In this letter, we introduce *dynamical cancellation* (DynaCan), a method to suppress adverse, pulse-induced transient eddy currents. DynaCan exploits the fact that eddy currents are typically a superposition of modes that decay exponentially with their individual time constants. Different time constants correspond to different spatial eddy-current patterns. An additional pulsed magnetic-field waveform with features at corresponding time scales thus allows selective coupling to the dynamics of the individual patterns. This cancellation pulse is provided by a current fed into a separate coil, spatially larger than the B_p coil, during the later part and turn off of the polarizing pulse. The computationally determined DynaCan current waveform is designed to drive the eddy currents to zero at the precise moment that the polarizing field becomes zero. As an example, preliminary simulations²⁰ with a simplified, spherically symmetric model of a shielded room demonstrated perfect cancellation of the 12 longest eddy-current time constants (Fig. 1). Here, we present an experimental implementation demonstrating a reduction of the eddy-current fields by 99%.

Figure 2 shows the Berkeley ULF-MRI system. The single-layer enclosure for attenuating external electromagnetic noise is a $(2.44\text{ m})^3$ cube constructed from 1.6-mm-thick

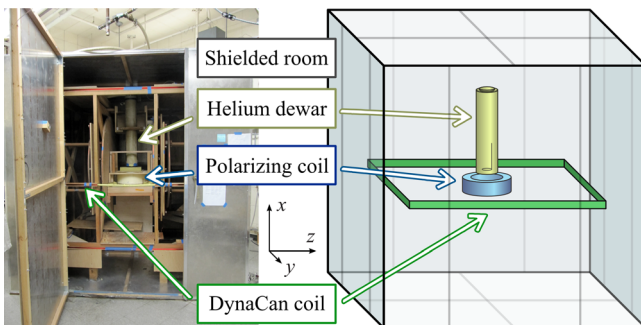


FIG. 2. Aluminum shielded room containing the detector and coils.

6061 aluminum sheets.¹⁹ The copper coils wound on wooden frames produce the static magnetic field, pulsed spin manipulation fields, the adiabatic sweep field,²⁰ and spatially encoding magnetic-field gradients for MRI, as described in detail elsewhere.^{20–23} The water-cooled B_p coil, consisting of 240 turns of $4 \times 4\text{ mm}^2$ hollow copper tubing, has an inner diameter of 324 mm, an outer diameter of 413 mm, and a height of 115 mm. The center of the coil is 1.14 m above the room floor and 1.30 m below the ceiling. The coil produces a field of 150 mT at its center in the vertical (x) direction with a 200-A current generated by a 20-kW power supply. This current is ramped to zero in 11.1 ms in a quarter-cosine waveform produced by insulated-gate bipolar transistors (IGBTs) and capacitors that form a resonant circuit with the coil.²⁴ The turn-off of the 150-mT B_p field generates a multi-exponentially decaying eddy-current transient with an initial amplitude of about $70\text{ }\mu\text{T}$ at the center of the room.¹⁹ Especially the two longest notable time constants—measured to be 6 ms and 23 ms—influence MRI measurements.

For DynaCan, we installed a square cancellation coil (Fig. 2) that is coaxial and coplanar with the B_p coil. The coil consists of 30 turns of 2.6-mm-diameter copper wire with a side length of 1.85 m, a resistance of $0.6\text{ }\Omega$, and an inductance of 5.9 mH. This configuration couples well to the eddy currents, but produces a field of only $18.3\text{ }\mu\text{T/A}$ at its center. The two ends of the B_p and DynaCan coils are connected to their respective power supplies via relays, situated just outside the shielded room, which open before data acquisition to prevent the coupling of electromagnetic interference into the measurement circuit.

To measure the transient magnetic field in the x direction with and without DynaCan, we used a single SQUID magnetometer in a low-noise fiberglass dewar (Fig. 2) containing liquid He at 4.2 K. The 7-mm-diameter superconducting pickup loop—a single turn of 120- μm -diameter Nb wire—was connected to the on-chip input coil of a dc SQUID.²⁵ The low-transition-temperature SQUID was surrounded by a superconducting Nb can. The pickup loop was at the center of the shielded room, 80 mm above the center of the B_p coil. The range of the magnetometer was about $\pm 620\text{ nT}$.

We now derive the theory for the practical implementation of DynaCan. If we model eddy currents as a superposition of spatial patterns with amplitudes given by the elements of a vector $\mathbf{j}(t)$, we can describe their excitation and dynamics by the linear system of differential equations,¹⁹

$$\mathbf{M} \frac{d\mathbf{j}}{dt} + \mathbf{R}\mathbf{j} + \mathbf{m} \frac{dI}{dt} = \mathbf{0}. \quad (1)$$

Here, the elements of the symmetric matrix \mathbf{M} are the mutual and self inductances of the spatial eddy-current patterns, and the matrix \mathbf{R} contains the resistances of the current patterns on its diagonal; the off-diagonal “mutual resistances” describe the ohmic coupling between patterns that share the same conductor. The third term is an electromotive force (EMF) induced by the current $I(t)$ in a coil, which couples to the eddy-current patterns via mutual inductances in the vector \mathbf{m} . A magnetic-field component B examined at a point of interest is affected by the eddy currents according to $B(t) = \boldsymbol{\beta}^\top \mathbf{j}(t)$,

where $\boldsymbol{\beta}$ is a coupling vector corresponding to the point and component of interest (\top denotes the transpose).

Whereas the adverse transients are large compared to the signal to be measured, they are small compared to the pulse that excites them. The eddy currents are thus best observed after the coil current is quickly brought to zero, as the magnetic fields produced by eddy currents then dominate a magnetic-field measurement. Assume, for now, a unit current in the coil, which is switched to zero at the instant $t = 0$:

$$I(t) = 1 - \theta(t). \quad (2)$$

Here, $\theta(t)$ is the Heaviside step function, the derivative of which is the Dirac delta $\delta(t)$, so that $dI/dt = -\delta(t)$. The resulting eddy currents $\mathbf{j}_{\text{ISR}}(t)$ cause a magnetic-field transient $B_{\text{ISR}}(t) = \boldsymbol{\beta}^\top \mathbf{j}_{\text{ISR}}(t)$, which we call the inverse-step response (ISR). The temporal Fourier transform (denoted by $\hat{\cdot}$) of Eq. (1) yields $i\omega \mathbf{M} \hat{\mathbf{j}}_{\text{ISR}} + \mathbf{R} \hat{\mathbf{j}}_{\text{ISR}} - \mathbf{m} = 0$, where ω is the angular frequency and we have used the fact that $\hat{\delta} = 1$. The frequency-domain solution for this case becomes

$$\hat{\mathbf{j}}_{\text{ISR}}(\omega) = (i\omega \mathbf{M} + \mathbf{R})^{-1} \mathbf{m}, \quad (3)$$

representing a multi-exponential decay in the time domain. Similarly, the frequency-domain equation for any applied current waveform $I(t)$ is $(i\omega \mathbf{M} + \mathbf{R}) \hat{\mathbf{j}} + i\omega \mathbf{m} \hat{I} = 0$, which has a solution,

$$\hat{\mathbf{j}} = -(i\omega \mathbf{M} + \mathbf{R})^{-1} \mathbf{m} \times i\omega \hat{I} = -\hat{\mathbf{j}}_{\text{ISR}} \times i\omega \hat{I}. \quad (4)$$

We simplified Eq. (4) using Eq. (3). The inverse Fourier transform turns the product into a convolution (denoted by $*$) in the time domain:

$$\mathbf{j}(t) = -\left(\mathbf{j}_{\text{ISR}} * \frac{dI}{dt}\right)(t). \quad (5)$$

Provided the field response $B_{\text{ISR}}(t)$ to an inverse step current [Eq. (2)] is known, the time evolution of the eddy-current field transient $B(t)$ caused by any pulse waveform $I(t)$ can be computed;

$$B(t) = -\left(B_{\text{ISR}} * \frac{dI}{dt}\right)(t). \quad (6)$$

Similarly, the field transient can be computed for any combination of a coil and field point (and component), provided the corresponding ISRs are available.

For DynaCan, we consider the polarizing and cancellation coils with currents $I_p(t)$ and $I_c(t)$. The coils have individual mutual inductances \mathbf{m}_p and \mathbf{m}_c with the eddy-current patterns, leading to corresponding ISRs $B_{\text{ISR}}^{(p)}$ and $B_{\text{ISR}}^{(c)}$. The third term in Eq. (1) becomes $\mathbf{m}_p dI_p/dt + \mathbf{m}_c dI_c/dt$, and the total field transient becomes

$$B_{\text{tr}}(t) = -\left[\left(B_{\text{ISR}}^{(p)} * \frac{dI_p}{dt}\right)(t) + \left(B_{\text{ISR}}^{(c)} * \frac{dI_c}{dt}\right)(t)\right]. \quad (7)$$

The principle of DynaCan is to design a current waveform $I_c(t)$ that ends at the same time as the polarizing current $I_p(t)$, at $t = 0$, and couples to the eddy currents so that they (and B_{tr}) are driven to zero at $t = 0$.

To implement this method, we obtained ISRs both from the theoretical model¹⁹—with 1536 eddy-current modes computed from the known geometry of the room and coils—and from measurements. The computational model worked well for time constants up to 6 ms, but the experimental response revealed an additional low-amplitude transient with a dominant time constant of about 23 ms. To measure the ISRs with the configuration described above, we used a ramp-down of 1 ms, which is a good approximation to an inverse step [Eq. (2)] for modes with time constants much longer than 1 ms. It is challenging (although possible¹⁹) to measure instantaneously after $t = 0$; in fact, the experimental ISRs began at about $t = 13$ ms. This was sufficient because shorter effects were already characterized by theory, and DynaCan can integrate information about multiple transients simultaneously.

To find the DynaCan waveform, we implemented an iterative optimization in Python using IPython²⁶ and numerical packages of the SciPy Stack. Since the duration of the waveform should be at least on the order of the longest transient time constant, we chose a duration of 40 ms. The waveform was represented by the first 40 coefficients of a sine series, and the optimization algorithm was set to minimize the integral of the square of the computed B_{tr} between $t = 3$ and 13 ms and of the measurement-based B_{tr} between $t = 13$ and 23 ms. The maximum voltage (ohmic and inductive) across the DynaCan coil for a full B_p amplitude (150 mT at the center) was constrained to 110 V to stay within amplifier capabilities. The resulting DynaCan waveform $I_c(t)$ per unit polarizing current is presented in Fig. 3.

To demonstrate DynaCan experimentally, we applied the pulses in Fig. 3. The duration of the B_p pulse was 120 ms and of the ramp-down 11.1 ms. The 40-ms compensation current waveform was supplied to the cancellation coil by a power amplifier in the controlled-current mode. The logic pulse for opening the mechanical relays in the B_p and DynaCan coil circuits was initiated at $t = 1$ ms (Fig. 3(a)),

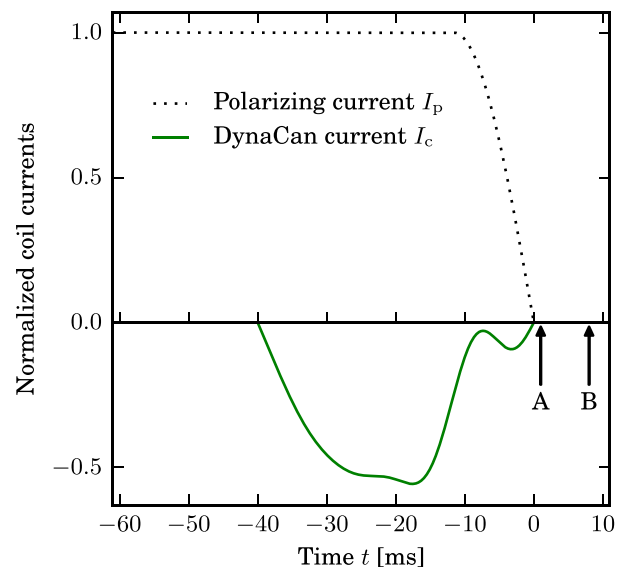


FIG. 3. Dynamical cancellation waveform I_c and end of polarizing pulse I_p ; the currents are normalized to the amplitude of I_p . Arrows indicate logic switching instants for (a) opening relays in the B_p and DynaCan coil circuits and (b) beginning data acquisition.

and the magnetometer began acquiring data at $t = 8$ ms when the mechanical relays had opened (Fig. 3(b)).

Without DynaCan, to record the eddy-current transients within the range of the magnetometer, we reduced the B_p current strength I_p from 200 A to three different values, 6.2, 8.3, and 9.8 A. The DynaCan waveform was scaled correspondingly. The magnetic-field transients (Fig. 4) were averaged over 200 runs to reduce interference at 60 Hz and its harmonics. In the absence of DynaCan, following the enabling of the magnetometer at 8 ms, the eddy currents generated magnetic fields of 318, 414, and 494 nT. In contrast, applying the computed waveform in the DynaCan coil suppressed the transients by two orders of magnitude to maximum values of 2.7, 4.1, and 5.0 nT. The transients in Figs. 4(a), 4(b), and 4(c) were thus canceled by 99.2%, 99.0%, and 99.0%, respectively.

The accuracy of the cancellation was limited by the uncertainty in the B_p current, engendered by the variation (about 1%) in the voltage produced by our power supply and switching electronics. In addition, the cancellation pulse has a small effect on the polarizing pulse waveform because of the mutual inductance between the two coils. If necessary, the latter problem could be solved by adding one or more turns around the polarizing coil—in series with the DynaCan

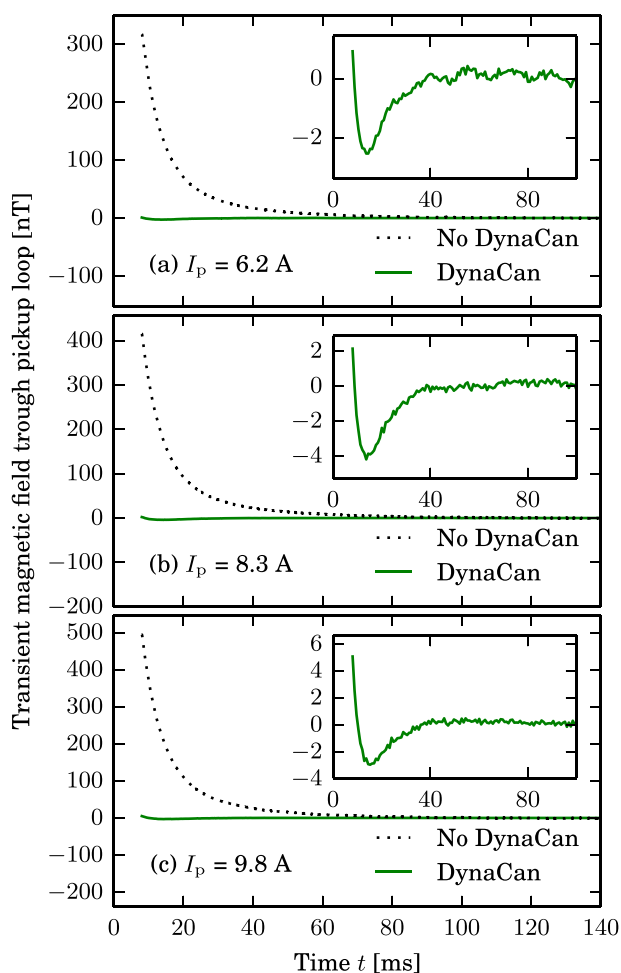


FIG. 4. Magnetic-field transients at the center of the room without (black) and with DynaCan (green, also in insets) for three different B_p currents I_p : (a) 6.2 A, (b) 8.3 A, and (c) 9.8 A. Oscillations in the inset to (a) are residual 60-Hz interference.

coil—similar to the way that the adiabatic sweep coil in ULF MRI is decoupled from the main field coil.²⁰ Alternatively, a precise polarizing pulse current could be provided by a controlled-current amplifier. To avoid additional transients due to mutual inductances with other coils, we disconnected all the MRI coils except the B_p and DynaCan coils. In general, minor coil-to-coil coupling issues can be solved using fast, low-noise ULF-MRI current sources.²⁷

If both I_p and I_c were supplied by amplifiers with stable properties, DynaCan could be fine-tuned to even higher accuracy. For increased cancellation accuracy, however, the computed DynaCan waveforms typically contain more oscillations towards the end. These oscillations accumulate more error from the ISRs and may not initially lead to increased accuracy. To improve the accuracy, one could implement a multi-pass procedure, in which the measured residual transient is fed back into the waveform optimization as the transient to be canceled. This procedure could iterate out the effects of inaccuracies not only in the ISRs but also in the theory, for instance, if the dynamics were slightly nonlinear.

Indeed, while the theory presented here is for a linear system of eddy currents [Eq. (1)], the transient need not necessarily be linear or even due to eddy currents. For instance, transients in electronics or in mechanical structures could be eliminated. Even the in-sequence demagnetization of a superconducting B_p coil, demonstrated recently,²⁸ can also be interpreted as an instance of nonlinear DynaCan. It is also possible to cancel multiple superposed transients simultaneously. In fact, the additional effects with time constants greater than 6 ms appear not to be eddy currents in the shielded room, but rather a transient in nearby structures such as the steel-reinforced concrete floor.

Dynamical cancellation provides an accurate, effective, and flexible way to eliminate harmful transients once sufficient information about the pulse-induced responses is available from modeling or measurements. Notably, a waveform completely different from the polarizing pulse produces excellent cancellation of the transient. This is because the geometrical complexity of the eddy currents is dealt with by the computer-generated temporal complexity of the DynaCan waveform. This has the great advantage that, for a given set of system hardware parameters, the cancellation can be optimized in software. We have developed a method for optimizing the cancellation waveform and demonstrated DynaCan experimentally, suppressing the eddy-current transients by 99%. Finally, DynaCan should also be applicable, for example, to magnetorelaxometry²⁹ and to magnetically shielded rooms comprising layers of high-permeability alloy.

H.D. and J.C. gratefully acknowledge the Henry H. Wheeler, Jr., Brain Imaging Center and the Donaldson Trust for support. R.J.I. and K.C.J.Z. thank the Academy of Finland, the Finnish Cultural Foundation, the International Doctoral Programme in Biomedical Engineering and Medical Physics (iBioMEP), and the European Community's Seventh Framework Programme (FP7/2007–2013) under Grant Agreement No. 200859 for funding this research.

¹R. McDermott, S.-K. Lee, B. ten Haken, A. H. Trabesinger, A. Pines, and J. Clarke, *Proc. Natl. Acad. Sci. U.S.A.* **101**, 7857 (2004).

- ²M. Möhle, S.-I. Han, W. R. Myers, S.-K. Lee, N. Kelso, M. Hatridge, A. Pines, and J. Clarke, *J. Magn. Reson.* **179**, 146 (2006).
- ³J. Clarke, M. Hatridge, and M. Möhle, *Annu. Rev. Biomed. Eng.* **9**, 389 (2007).
- ⁴V. S. Zotev, A. N. Matlashov, P. L. Volegov, A. V. Urbaitis, M. A. Espy, and R. H. Kraus, Jr., *Supercond. Sci. Technol.* **20**, S367 (2007).
- ⁵H. Dong, L. Qiu, W. Shi, B. Chang, Y. Qiu, L. Xu, C. Liu, Y. Zhang, H.-J. Krause, A. Offenhäusser, and X. Xie, *Appl. Phys. Lett.* **102**, 102602 (2013).
- ⁶I. Hilschenz, R. Koerber, H.-J. Scheer, T. Fedele, H.-H. Albrecht, A. M. Cassará, S. Hartwig, L. Trahms, J. Haase, and M. Burghoff, *Magn. Reson. Imaging* **31**, 171 (2013).
- ⁷R. H. Kraus, Jr., M. A. Espy, P. E. Magnelind, and P. L. Volegov, *Ultra-Low Field Nuclear Magnetic Resonance* (Oxford, New York, 2014).
- ⁸S. K. Lee, M. Möhle, W. Myers, N. Kelso, A. H. Trabesinger, A. Pines, and J. Clarke, *Magn. Reson. Med.* **53**, 9 (2005).
- ⁹S. Busch, M. Hatridge, M. Möhle, W. Myers, T. Wong, M. Mück, K. Chew, K. Kuchinsky, J. Simko, and J. Clarke, *Magn. Reson. Med.* **67**, 1138 (2012).
- ¹⁰I. Nestrail, S. Michaeli, T. Liimatainen, C. E. Rydeen, C. M. Kotz, J. P. Nixon, T. Hanson, and P. J. Tuite, *J. Neurol.* **257**, 964 (2010).
- ¹¹M. Haris, A. Singh, K. Cai, C. Davatzikos, J. Q. Trojanowski, E. R. Melhem, C. M. Clark, and A. Borthakur, *J. Neurol.* **258**, 380 (2011).
- ¹²H. I. Mäkelä, E. De Vita, O. H. J. Gröhn, M. I. Kettunen, M. Kavec, M. Lythgoe, M. Garwood, R. Ordidge, and R. A. Kauppinen, *Magn. Reson. Med.* **51**, 4 (2004).
- ¹³V. S. Zotev, A. N. Matlashov, P. L. Volegov, I. M. Savukov, M. A. Espy, J. C. Mosher, J. J. Gomez, and R. H. Kraus, Jr., *J. Magn. Reson.* **194**, 115 (2008).
- ¹⁴P. T. Vesänen, J. O. Nieminen, K. C. J. Zevenhoven, J. Dabek, L. T. Parkkonen, A. V. Zhdanov, J. Luomahaara, J. Hassel, J. Penttilä, J. Simola, A. I. Ahonen, J. P. Mäkelä, and R. J. Ilmoniemi, *Magn. Reson. Med.* **69**, 1795 (2013).
- ¹⁵M. E. Packard and R. Varian, *Phys. Rev.* **93**, 941 (1954).
- ¹⁶J. O. Nieminen, P. T. Vesänen, K. C. J. Zevenhoven, J. Dabek, J. Hassel, J. Luomahaara, J. Penttilä, and R. J. Ilmoniemi, *J. Magn. Reson.* **212**, 154 (2011).
- ¹⁷S.-M. Hwang, K. Kim, C. S. Kang, S.-J. Lee, and Y.-H. Lee, *Appl. Phys. Lett.* **99**, 132506 (2011).
- ¹⁸S.-M. Hwang, K. Kim, C. S. Kang, S.-J. Lee, and Y.-H. Lee, *J. Appl. Phys.* **111**, 083916 (2012).
- ¹⁹K. C. J. Zevenhoven, S. Busch, M. Hatridge, F. Öisjöen, R. J. Ilmoniemi, and J. Clarke, *J. Appl. Phys.* **115**, 103902 (2014).
- ²⁰K. Zevenhoven, "Solving transient problems in ultra-low-field MRI," M.Sc. thesis (Aalto University, Helsinki, 2011), available at <http://urn.fi/URN:NBN:fi:aalto-201305163099>.
- ²¹R. McDermott, N. Kelso, S.-K. Lee, M. Möhle, M. Mück, W. Myers, B. ten Haken, H. C. Seton, A. H. Trabesinger, A. Pines, and J. Clarke, *J. Low Temp. Phys.* **135**, 793 (2004).
- ²²W. R. Myers, "Potential applications of microtesla magnetic resonance imaging detected using a superconducting quantum interference device," Ph.D. dissertation, University of California, Berkeley, 2006.
- ²³B. Inglis, K. Buckenmaier, P. SanGiorgio, A. F. Pedersen, M. A. Nichols, and J. Clarke, *Proc. Natl. Acad. Sci. U.S.A.* **110**, 19194 (2013).
- ²⁴N. I. Matter, G. C. Scott, T. Grafendorfer, A. Macovski, and S. M. Conolly, *IEEE Trans. Med. Imaging* **25**, 84 (2006).
- ²⁵STAR Cryoelectronics, 25-A Bisbee Court, Santa Fe, NM 87508-1412.
- ²⁶F. Pérez and B. E. Granger, *Comput. Sci. Eng.* **9**, 21 (2007).
- ²⁷K. C. J. Zevenhoven and S. Alanko, *J. Phys.: Conf. Ser.* **507**, 042050 (2014).
- ²⁸K. C. J. Zevenhoven, J. O. Nieminen, J. Dabek, P. T. Vesänen, L. T. Parkkonen, J. Simola, A. I. Ahonen, and R. J. Ilmoniemi, "Towards high-quality ultra-low-field MRI with a superconducting polarizing coil," paper presented at the 11th European Conference on Applied Superconductivity (EUCAS 2013), Abstract 3A-EL-O4, 18 September 2013.
- ²⁹J. Lange, R. Kötz, A. Haller, L. Trahms, W. Semmler, and W. Weitschies, *J. Magn. Magn. Mater.* **252**, 381 (2002).